analytical chemistry

Article

Cite This: *Anal. Chem.* 2018, 90, 2618−2624

pubs.acs.org/ac

MnO_2 Nanosheet-Carbon Dots Sensing Platform for Sensitive Detection of Organophosphorus Pesticides

Xu Yan,*[,†,‡,§,¶] Yang Song,[‡,¶] Chengzhou Zhu,[‡] Hongxia Li,[†] Dan Du,[‡] Xingguang Su,*[,§] and Yuehe Lin*[,‡]

[†]State Key Laboratory on Integrated Optoelectronics, College of Electron Science and Engineering, Jilin University, 2699 Qianjin Street, Changchun 130012, China

[‡]School of Mechanical and Materials Engineering, Washington State University, Pullman, Washington 99164, United States

[§]Department of Analytical Chemistry, College of Chemistry, Jilin University, 2699 Qianjin Street, Changchun 130012, China

Supporting Information

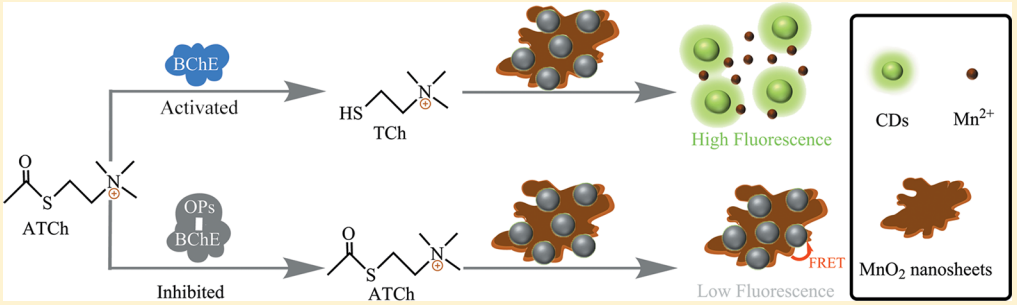

ABSTRACT: Carbon dots (CDs) combined with a nanomaterial-based quencher has created an innovative way for designing promising sensors. Herein, a novel fluorescent-sensing platform was designed for sensitive detection of organophosphorus pesticides (OPs). The preparation of CDs was based on one-step hydrothermal reaction of 3-aminobenzeneboronic acid. The fluorescence of CDs can be quenched by manganese dioxide (MnO_2) nanosheets via the Förster resonance energy transfer (FRET). In the presence of butyrylcholinesterase (BChE) and acetylthiocholine, the enzymatic hydrolysate (thiocholine) can efficiently trigger the decomposition of MnO_2 nanosheets, resulting in the recovery of CDs fluorescence. OPs as inhibitors for BChE activity can prevent the generation of thiocholine and decomposition of MnO_2 nanosheets, accompanying the fluorescence "turn-off" of the system. So the BChE-ATCh-MnO_2−CDs system can be utilized to detect OPs quantitatively based on the fluorescence turn "on−off". Under the optimum conditions, the present FRET-based approach can detect paraoxon ranging from 0.05 to 5 ng mL^{-1} with a detection limit of 0.015 ng mL^{-1}. Meanwhile, the present strategy also showed a visual color change in a concentration-dependent manner. Thus, the proposed assay can potentially be a candidate for OPs detection.

Pesticides are essential substances for crop growth and storage via controlling pests in modern commercial agriculture.[1,2] Organophosphorus pesticides (OPs) are a significant type of pesticide which have been extensively utilized across the world due to their relatively high effectiveness and low persistence.[3,4] However, the improper disposal and residues of OPs result in serious contamination of agricultural products and the environment.[5] In particular, OPs act as a neurotoxin by impeding the activity of cholinesterase at very low concentrations, causing damage to human health or even fatal consequences.[6,7] Therefore, the detection and monitoring of OPs has become increasingly important because it concerns human health. Many sensing methods have been designed to detect OPs, including chemiluminescence,[8] electrochemical assay,[9] and enzyme-linked immunosorbent assay.[10,11] However, several disadvantages of the mentioned methods still exist, such as complicated modifications of the electrode, dependence on professional technology, sophisticated instruments, and the necessity of the specific antibody to a pesticide, causing these strategies to have limited application.[12−14] Accordingly, the development of a new sensing platform for OPs is highly desirable to facilitate routine analysis. Recently, a fluorescence-based strategy has been considered a promising method, owing to its high sensitivity and selectivity.[15,16] Fluorescent carbon dots (CDs) as promising carbon nanomaterial candidates have inspired extensive studies owing to their superior merits of easy preparation, low biological toxicity, good biocompatibility, and unique photoluminescent behavior.[17−19] Compared to conventional dye molecules, quantum dots and metal clusters, CDs possess distinct advantages, such as excellent biocompatibility, low photobleaching, and good water solubility.[20,21] More

Received: October 12, 2017
Accepted: December 14, 2017
Published: December 14, 2017

DOI: 10.1021/acs.analchem.7b04193
Anal. Chem. 2018, 90, 2618−2624

Scheme 1. Schematic Illustration of Sensing Strategy for OPs Detection Based on CDs-MnO_2 Nanosheets

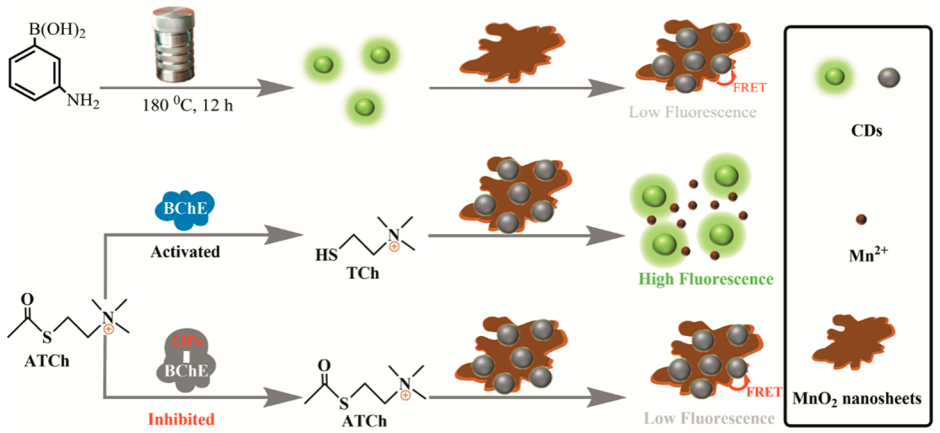

importantly, CDs have many more sources of raw materials and various approaches, which make the synthesis of CDs easier. These outstanding properties endowed CDs with potential applications in numerous fields, such as sensing,[22] catalysis,[23] bioimaging,[24] and drug delivery.[25]

Combinations of fluorescent probes and nanomaterial-based quenchers in a sensing system have been widely utilized for designing promising sensors. To date, graphene oxide,[26] metal nanoparticles,[27,28] and transition-metal dichalcogenides[29,30] have been employed as efficient quenchers to establish fluorescent-sensing platforms. However, the synthesis condition of these nanomaterials was sophisticated and strict. In addition, some of these nanomaterials display biological toxicity.[31] Manganese dioxide (MnO_2) nanosheets, as a kind of two-dimensional nanomaterial, have received extensive investigative attention because of their high specific surface area, superior light absorption capability, and good environmental compatibility.[32−34] Moreover, MnO_2 nanosheets have oxidation ability and can be converted to Mn^{2+} by reductive species. These properties allow MnO_2 nanosheets to serve as nanoquenchers,[35−37] catalysts,[38,39] adsorbents,[40] and so on. For example, Liu's group first prepared MnO_2-nanosheet-modified upconversion nanoparticles for intracellular glutathione (GSH) detection.[35] Thereafter, Cai et al. designed a facile fluorescence "switch-on" strategy for measuring GSH by utilizing MnO_2−CDs nanocomposite.[41] In Mao's system, 7-hydroxycoumarin worked as a fluorescence reporter for ascorbic acid detection based on the static quenching effect and inner filter effect between the fluorophore and MnO_2 nanosheets.[42] Lin's group developed a rapid sensing platform employing CDs and MnO_2 nanosheets for the determination of GSH in human blood sample.[43]

Enlightened by the aforementioned work, by employing the enzyme of BChE with specific recognition and the excellent inhibition effect of OPs, we herein developed a facile fluorescence platform for the sensitive detection of OPs by utilizing MnO_2−CDs nanosensor. As shown in Scheme 1, the ultrathin MnO_2 nanosheets as energy acceptor can turn off the fluorescence (FL) intensity of CDs via Förster resonance energy transfer (FRET). Interestingly, the MnO_2 nanosheet-induced quenching effect can be recovered by adding BChE and acetylthiocholine (ATCh) to the sensing system. OPs as inhibitor to suppress BChE activity can decrease the decomposition of MnO_2, resulting in the fluorescence quenching again. The FL signal change was corresponding to OPs-induced inhibition reaction. In this sensing platform, MnO_2 nanosheets served as both nanoquencher and recognition unit for quantitative detection of OPs with outstanding sensitivity. The proposed MnO_2-based nanosensor overcame the disadvantage of relatively poor monodispersity in an aqueous solution of MnO_2-fluorophore composites.[35,41] Meanwhile, the precise specificity of BChE and the pretreatment process of samples can also block the influence of other reducing agents, such as ascorbic acid,[42] GSH,[41,43] and dithiothreitol,[37] enhancing the selectivity of nanosensor. Furthermore, the designed nanosensor not only showed great potential in OPs monitoring but also displayed huge promise for evaluating OPs poisoning. This sensing system provided a new way for probing other reducing agent product-related enzyme system.

EXPERIMENTAL SECTION

Reagents and Instruments. $KMnO_4$, sodiumdodecyl sulfate, butyrylcholinesterase (BChE, ≥ 300 U mg^{-1} protein from equine serum), acetylthiocholine (ATCh) iodide (≥98%), paraoxon, and 3-aminobenzeneboronic acid of analytical grade were obtained from Sigma-Aldrich Corporation. The water had a good resistivity (>18MΩ cm^{-1}) in this work. The FL spectra and UV−vis spectra were collected by Cary Eclipse fluorimeter and UV-2450 spectrometer, separately. Transmission electron microscopy (TEM) images were measured by a Philips CM200UT transmission electron microscope.

Preparation of CDs. 3-Aminobenzeneboronic acid (0.1 g) was dissolved in 10.0 mL of DI water and then was transferred into polytetrafluoroethylene autoclaves. After heating the solution at 180 °C for 12 h, a yellow-green solution was obtained. The solution was purified with a dialysis bag (MWCO ∼ 1.0 kDa) and dialyzed for 2 days to remove small molecules. Finally, CDs were freeze-dried to a yellow-green solid.

Preparation of MnO_2 Nanosheets. Ultrathin MnO_2 nanosheets were synthesized as in the previous study.[32] Briefly, 0.1 mol L^{-1} of sodium dodecyl sulfate solution (5 mL), 0.1 mol L^{-1} of H_2SO_4 solution (250 μL), and 44.25 mL distilled water were mixed together, then heated at 95 °C for 15 min. 0.05 mol L^{-1} of $KMnO_4$ solution (500 μL) was added into above solution for another 60 min. The synthesized MnO_2 nanosheets were purified by repeated washing with ultrapure

DOI: 10.1021/acs.analchem.7b04193
Anal. Chem. 2018, 90, 2618−2624

water. Finally, MnO_2 nanosheets were freeze-dried to a brownish black powder.

Detection Procedure for BChE. Various concentrations of BChE (50 μL) were mixed with 10 mmol L^{-1} of ATCh (50 μL) and 10 mmol L^{-1} of PBS (pH = 8.5, 50 μL) for 20 min at 37 °C. Then, 150 μL of MnO_2 nanosheets (1 mg mL^{-1}) and 20 μL of CDs (200 μg mL^{-1}) were added to the solution. The mixtures were diluted to 500 μL with ultrapure water and mixed thoroughly before the fluorescence spectra were collected.

Procedures for OPs Sensing. Paraoxon was selected as a model analyte to inhibit BChE activity. The paraoxon standard substance were dissolved in PBS buffer solution (10.0 mmol L^{-1}, pH = 7.4) containing 5% ethanol for preparing the standard solution. Different concentrations of standard solution (25 μL) and 10 μg mL^{-1} of BChE (25 μL) were mixed at 37 °C for 30 min. Then, 10 mmol L^{-1} of ATCh (50 μL) and 10 mmol L^{-1} of PBS (pH = 8.5, 50 μL) were added and incubated at 37 °C for 20 min. Next, 150 μL of MnO_2 nanosheets (1 mg mL^{-1}), 20 μL of CDs (200 μg mL^{-1}) and 280 μL of ultrapure water were added. After 2.0 min of incubation, the fluorescence spectra were recorded.

RESULTS AND DISCUSSION

Characterization of CDs and MnO_2 Nanosheets. The CDs were prepared by a green route, one-step hydrothermal reaction of 3-aminobenzeneboronic acid. The morphology of CDs was characterized by transmission electron microscopy (TEM). The results (Figure 1A) illustrated that the CDs were near spherical with good dispersion and fairly uniform in size (average size 3 nm). The optical properties of the CDs were investigated by UV−vis absorption and fluorescence spectra. The characteristic absorption peak around 330 nm found in the UV−vis spectra was due to the n−π^* transition of C═O and π−π^* transition of C═C (Figure 1B). Similar to most carbon nanomaterials, the CDs showed an excitation-dependent FL behavior due to the surface defects and size distribution of CDs. As shown in Figure 1C, when the excitation wavelength was changed from 360 to 460 nm, the FL peak correspondingly shifted from 493 to 534 nm, accompanied by the increase of FL intensity and then decrease. Moreover, CDs exhibited the maximum fluorescence emission at 504 nm with excitation wavelength at 400 nm. The chemical stability and photostability of CDs is critical for its practical applications. The FL intensity of CDs under 400 nm excitation gradually increases with the pH values increase from 5.5 to 7.0 and then slowly decreases with further increasing the pH values (as depict in Figure 1D), implying the best FL performance in neutral solution. The stability of the prepared CDs under different concentration of salt was investigated. It is obviously shown in Figure 1E that the fluorescence of CDs remains almost constant in a wide salt concentration range of 0−10 mmol L^{-1}. For photostability, we utilized a 250 W xenon lamp for continuous intensive excitation for 60 min, and we obtained the photobleaching curves of CDs. From Figure 1F, we clearly observed that the FL emission intensity of CDs preserved ∼30% of the initial intensity after 60 min of xenon lamp irradiation, while CdTe quantum dots (QDs) quickly quenched due to photobleaching within 10 min, indicating that the CDs exhibit better photostability compared to that of QDs. The results indicate that as-prepared CDs had good stability, making them promising as a fabrication sensor.

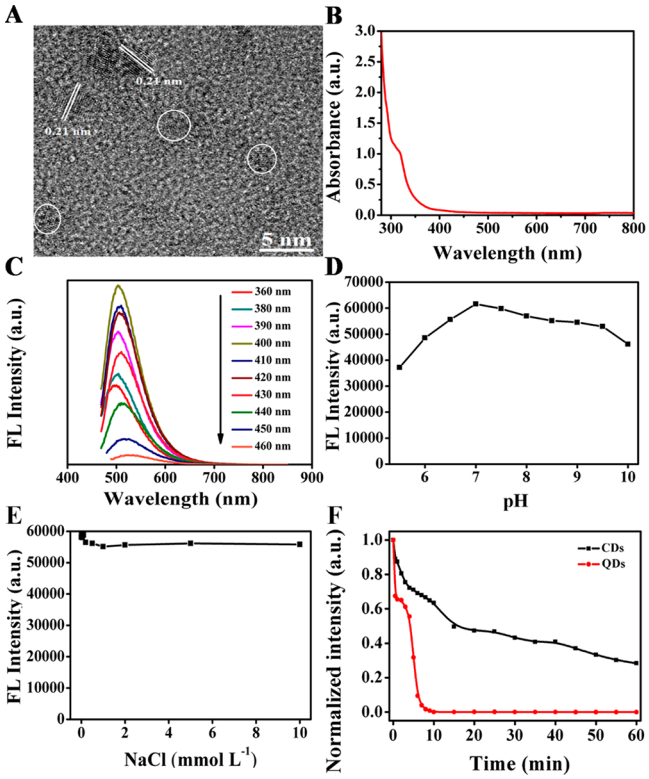

Figure 1. (A) TEM image of the CDs. (B) UV−vis absorption spectrum of CDs. (C) FL emission spectra of the CDs recorded at various excitation wavelengths in the range from 360 to 460 nm. (D) Effect of pH on the FL intensity of CDs. (E) Effect of NaCl concentration on the FL intensity of CDs. (F) Photobleaching experiment of the CDs and CdTe QDs with a 250 W xenon lamp for continuous intensive excitation.

The ultrathin MnO_2 nanosheets, which served as dual-functional nanoquencher and recognizer, were prepared through a redox reaction between SDS and $KMnO_4$. MnO_2 nanosheets were first confirmed by TEM and UV−vis spectroscopy. The MnO_2 nanosheets showed two-dimensional structure with the average lateral dimension of nearly 100 nm in Figure 2A. Furthermore, MnO_2 nanosheets have a broad UV−vis absorption spectrum in the range from 300 to 500 nm (Figure 2B). Detailed analysis based on Raman spectra and X-ray photoelectron spectroscopy (XPS) was further investigated to confirm the features of MnO_2 nanosheets. As shown in Figure 2C, the Raman spectrum of the MnO_2 nanosheets showed two distinct peaks at 565.3 and 653.8 cm^{-1}, which was accredited to the Mn−O stretching vibration. Figure 2D displayed the XPS spectrum for the MnO_2 nanosheets. Two peaks located at 642.0 and 653.6 eV were detected and attributed to $Mn_{2p3/2}$ and $Mn_{2p1/2}$ of MnO_2, respectively. Thus, the aforementioned characterizations have demonstrated the successful preparation of MnO_2 nanosheets.

Design of MnO_2−CDs Platform. The designed biosensor consists of CDs and MnO_2 nanosheets, where CDs were served as fluorescence reporter, and MnO_2 nanosheets were employed as a dual-functional FL nanoquencher and recognizer. As shown in Figure 3A, CDs perform a maximum fluorescent signal at 504 nm under the excitation of 400 nm (curve a). The FL intensity of CDs can be significantly quenched by MnO_2 nanosheets through the FRET effect (curve b). Importantly, the quenched FL intensity can be

DOI: 10.1021/acs.analchem.7b04193
Anal. Chem. 2018, 90, 2618−2624

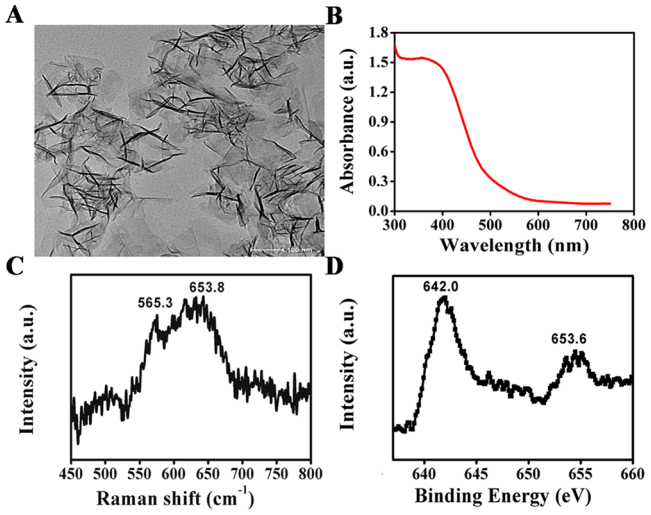

Figure 2. (A) TEM image of MnO_2 nanosheets. (B) UV−vis absorption spectra of MnO_2 nanosheets. (C) Raman spectrum of MnO_2 nanosheets and (D) XPS spectra of MnO_2 nanosheets.

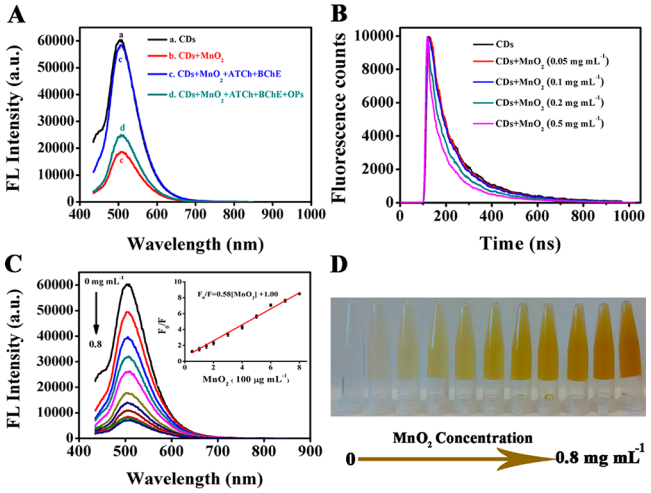

Figure 3. (A) FL spectra of CDs, CDs+MnO_2 nanosheets, CDs +MnO_2 nanosheets+BChE, CDs+ MnO_2 nanosheets+BChE+OPs. Final concentrations of CDs, MnO_2 nanosheets, BChE, and OPs are 8.0, 0.3, 0.5, and 0.025 μg mL^{-1}. (B) Lifetime of CDs in the absence and presence of MnO_2. (C) FL spectra of CDs in the presence of various concentrations of MnO_2 nanosheets (0, 0.05, 0.1, 0.15, 0.2, 0.3, 0.4, 0.5, 0.6, 0.7, and 0.8 mg mL^{-1}). Inset was the linear plot of F/F_0 versus the concentration of MnO_2 nanosheets. F and F_0 were the FL intensity of the CDs system in the presence and absence of MnO_2 nanosheets, respectively. (D) Corresponding photographs of the detection system taken under daylight.

recovered by introducing BChE and ATCh (curve c). BChE can catalytically hydrolyze ATCh to yield thiocholine (TCh), which can induce decomposition of the MnO_2 nanosheets (Figure S1), resulting in recovery of CDs fluorescence. As shown in eq 1, MnO_2 nanosheets were reduced to produce Mn^{2+}.

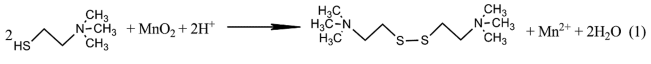

The reduction product Mn^{2+} was further verified by a highly specific reaction with IO_4^- (Figure S2). Paraoxon, as inhibitor to suppress the activity of BChE, could decrease the decomposition of MnO_2, leading to the fluorescence quenching again (curve d, Figure 3A). The CDs were also separately incubated with BChE, ATCh, or paraoxon under the same conditions (Figure S3). The results indicated that the FL intensity of CDs+BChE, CDs+ATCh, and CDs+paraoxon system was identical to that of CDs. All of the above results indicated that the detection principle for OPs is feasible.

According to previous reports, MnO_2 nanosheets as an efficient nanoquencher can obviously quench the FL of CDs via FRET.[41,43,44] In order to elucidate the underlying mechanism of MnO_2-induced fluorescence quenching, the fluorescence emission spectrum of CDs and the absorption spectrum of the MnO_2 nanosheets were first investigated. The absorbance band of MnO_2 nanosheets possessed overlap with the emission of CDs, which is highly beneficial to the formation of a FRET sensing strategy (see Figure S4A in the Supporting Information). Meanwhile, the MnO_2 nanosheets were negatively charged (ζ = −32.7) while CDs were positively charged (ζ = 10.3) (Figure S4B). In the presence of CDs, the zeta potential showed a significant reduction from −32.7 mV (MnO_2 nanosheets) to −20.4 mV (MnO_2 nanosheets-CDs system), indicating intensive electrostatic interaction between MnO_2 nanosheets and CDs which shortens the distance of nanomaterials to generate the FRET donor−acceptor pair. In addition, owing to the electrostatic interaction between MnO_2 nanosheets and CDs, the absorption spectrum of MnO_2 nanosheets and CDs mixture display a blue shift compared to that of MnO_2 nanosheets (Figure S4C). More importantly, the FL lifetime of CDs system in the presence of different concentration of MnO_2 nanosheets were studied (Figure 3B). The decay components and their ratios for the FL lifetime of CDs and CDs-MnO_2 system were shown in Table S1. The fluorescence decay curve was fitted by using a double exponential function including 7.64 ns (84.41%) and 1.23 ns (15.59%), respectively, and the average lifetime was 6.64 ns. With the increasing MnO_2 nanosheet concentration from 0 to 0.5 mg mL^{-1}, the lifetimes of CDs-MnO_2 system were gradually decreased from 6.64 to 4.58 ns, implying that the dynamic quenching process was dominant for the quenching mechanism. The corresponding quenching performances of MnO_2 nanosheets (0.05, 0.1, 0.2, and 0.5 mg mL^{-1}) toward CDs were also studied (Figure S5A). The fluorescence quenching efficiency can reach 82% after incubation with 0.5 mg mL^{-1} MnO_2 nanosheets (Figure S5B). The excellent energy transfer efficiency is attributed to the stronger optical absorption and larger surface area of MnO_2 nanosheets. As expected, with the increase in concentration of MnO_2 nanosheets (0−0.8 mg mL^{-1}), the FL emission intensity of CDs decreases gradually (Figure 3C). It can be obviously seen that the color of CDs-MnO_2 solution became deeper as the concentration of MnO_2 nanosheets increased (Figure 3D). Therefore, the FL intensity of the CDs can be quenched by MnO_2 nanosheets via the FRET effect.

BChE-Induced FL Quenching. In this sensing platform, CDs and MnO_2 nanosheets were employed as FRET donor−acceptor pair. BChE (0.1 μg mL^{-1}) was used to optimize the concentration of MnO_2 nanosheets and CDs (Figure S6). It could be observed that high FL intensity ratio (F_B/F_{B0}) was obtained with 0.3 mg mL^{-1} of MnO_2 nanosheets and 8.0 μg mL^{-1} of CDs. F_B and F_{B0} were the FL intensity of the ATCh-MnO_2−CDs system in the presence and absence of BChE, respectively.

DOI: 10.1021/acs.analchem.7b04193
Anal. Chem. 2018, 90, 2618−2624

To demonstrate the usability of this sensing platform for sensitive detection of OPs, we systematically tested the response of the system to different concentrations of BChE. As shown in Figure 4A, the FL intensity of CDs at 504 nm

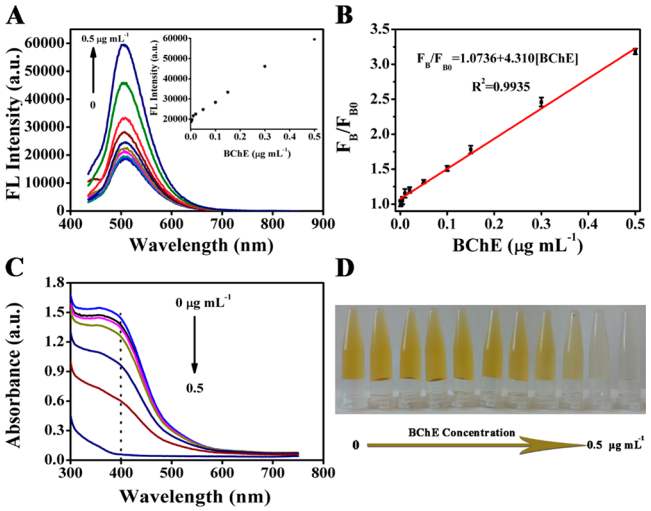

Figure 4. (A) FL spectra of MnO_2−CDs system with various concentrations of BChE. Final concentrations of BChE are 0, 0.001, 0.002, 0.005, 0.01, 0.02, 0.05, 0.1, 0.15, 0.3, and 0.5 μg mL^{-1}, respectively. Inset shows the change trend of the FL intensities with various concentrations of BChE. (B) Linear plot of (F_B/F_{B0}) versus the concentration of BChE. (C) UV−vis absorption spectra of sensing system in the presence of different concentration of BChE (0, 0.02, 0.05, 0.1, 0.15, 0.3, and 0.5 μg mL^{-1}). F_B and F_{B0} were the FL intensity of the MnO_2−CDs system in the presence and absence of BChE, respectively. (D) Corresponding photographs of the detection system taken under daylight.

recovered gradually with BChE concentration increasing from 0 to 0.5 μg mL^{-1}. Inset shows the FL intensities of CDs in the presence of different concentrations of BChE. A good linear relationship between F_B/F_{B0} and BChE concentration was obtained in the range from 0.001 to 0.5 μg mL^{-1}. The regression equation is F_B/F_{B0} = 1.0736 + 4.310 [BChE], μg mL^{-1} (Figure 4B). The corresponding regression coefficient is 0.9935, and the limit of detection (LOD) for BChE is 0.45 ng L^{-1} (signal-to-noise ratio of 3).[45] The decomposition of MnO_2 nanosheets was also confirmed by UV−vis absorption of the sensing system in the presence of different concentrations of BChE (Figure 4C). It can be clearly seen that with the increasing of BChE concentration, the absorption of MnO_2 at 400 nm decreased gradually, indicating that the destruction of MnO_2 nanosheets.

Moreover, there was also a color change from brown to colorless with the increase of BChE concentration in the sensing system (Figure 4D). Thus, a facile and low-cost colorimetric and fluorescent-sensing platform was developed for BChE activity detection. The concentrations of BChE have an influence on the hydrolysis of ATCh and consequently affect the decomposition of MnO_2 nanosheet and the FL intensity of CDs-based system. To obtain high sensitivity, 0.5 μg mL^{-1} of BChE was selected for OPs detection (Figure S7).

Sensitive Detection of Paraoxon. Owing to the good performance of the BChE-ATCh-MnO_2−CDs system, the designed nanosensor was investigated in screening and detection of OPs. When paraoxon was introduced to the BChE-ATCh-MnO_2−CDs system, the enzymatic reaction was efficiently retarded,[46,47] leading to the quench of FL intensity. For paraoxon detection, the incubation time of OPs were optimized to gain the best sensitivity (Figure S8). Under the optimal conditions, different concentrations of paraoxon were first incubated with BChE (0.5 μg mL^{-1}) at 37 °C for 30 min and then introduced to the sensing system. With the increasing of paraoxon, the FL intensity was gradually quenched. Inset shows the change trend of FL intensity toward the concentration of paraoxon (Figure 5A). As shown in Figure

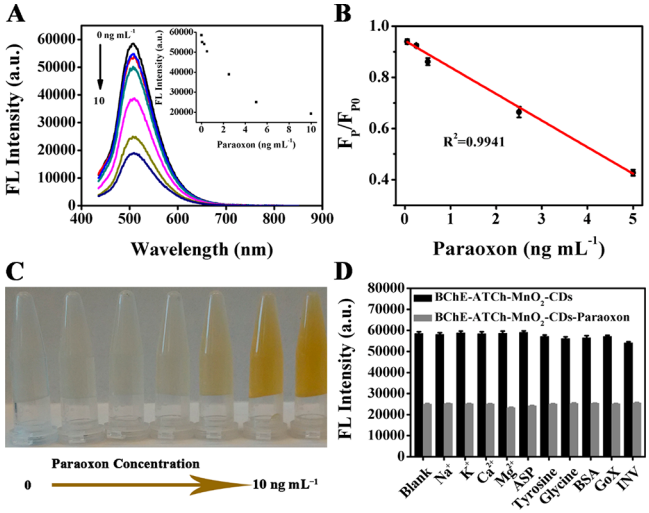

Figure 5. (A) FL spectra of the BChE-ATCh-MnO_2−CDs system with various concentration of paraoxon (0, 0.05, 0.25, 0.5, 2.5, 5.0, and 10 ng mL^{-1}). Inset illustrates the change trend of FL intensities with different concentrations of paraoxon. (B) Linear plot of F_P/F_{P0} toward the concentration of paraoxon. F_P and F_{P0} were the FL intensity of the BChE-ATCh-MnO_2−CDssystem in the presence and absence of paraoxon. (C) Corresponding photographs of the detection system taken under daylight. (D) FL intensity of the BChE-ATCh-MnO_2−CDs-paraoxon system with the interfering substances (5 μg mL^{-1}).

5B, A good linear relationship between F_P/F_{P0} and the concentrations of paraoxon (R^2 = 0.9941) was obtained in the range from 0.05 to 5 ng mL^{-1}. F_P and F_{P0} were the FL intensity of the BChE-ATCh-MnO_2−CDs system in the presence and absence of paraoxon, respectively. The regression equation is F_P/F_{P0} = 0.94308 (±0.00526) − 0.10401(±0.00267) [Paraoxon], ng mL^{-1}. The LOD for paraoxon is 0.015 ng mL^{-1} (signal-to-noise ratio of 3), which fulfill the determination requirements of paraoxon in food samples (the maximum residue limit of paraoxon in food is 10 ng mL^{-1}).[48] More importantly, there was a series of noticeable color changes from colorless to brown of BChE-ATCh-MnO_2−CDs solution with the increase of paraoxon concentration, indicating that the developed nanoprobe can be recognized by the naked eye for OPs detection (Figure 5C).

The related sensing methods for OPs detection with respect to linear range, sensitivity, and response time were summed up in Table S2. It could be observed that the sensitivity of this nanosensor was higher than many of the previous sensors. In previous studies, gold nanoparticle[49] and silver nanoparticle[50] were used as nanoquencher for the fabrication of OPs sensors. Those strategies can be easily influenced by chemicals, such as cyanide, salt, and melamine. In comparison with previous nanosensors, the MnO_2 nanosheets-based platform possesses high sensitivity and higher anti-interference ability. Further-

DOI: 10.1021/acs.analchem.7b04193
Anal. Chem. 2018, 90, 2618−2624

more, MnO_2 nanosheets showed a broad UV−vis absorption spectrum from 300 to 600 nm, suggesting that the nanosheets could be a versatile energy harvester for chromophores. MnO_2 nanosheets also can be reduced to Mn^{2+} ions by TCh, which may be friendly to the environment and human health.[34] More important, the response time was quite short or comparable in contrast with the existing enzyme-based assay methods. Therefore, the MnO_2 nanosheets-CDs sensing platform could be utilized for sensitive detection of paraoxon.

To illustrate that the proposed MnO_2 nanosheets-CDs system was functional not only for paraoxon but also for other OPs, we investigated the sensing platform for four common pesticide: parathion, chlorpyrifos, dichlorvos, and malathion. Figure S9 compared the FL intensity ratio (F_P/F_{P0}) of different pesticide at the concentration of 2.5 ng mL^{-1}. We observed that the F_P/F_{P0} values were 0.66, 0.69, 0.70, 0.75, and 0.79 for paraoxon, parathion, chlorpyrifos, dichlorvos, and malathion, indicating that the proposed platform can also be generally employed for monitoring OPs.

Selectivity is an important characteristic to evaluate the capability of the established nanosensor, especially for nanosensor in on-site applications. To evaluate the specificity of the sensing assay for paraoxon detection, the influence of some common electrolytes and biological species including Na^+, K^+, Ca^{2+}, Mg^{2+}, aspartic acid (ASP), tyrosine, glycine, bovine serum albumin (BSA), glucose oxidase (GoX), and invertase (INV) was investigated. As shown in Figure 5D, the BChE-ATCh-MnO_2−CDs system exhibited a remarkable increase of FL intensity toward paraoxon (5.0 ng mL^{-1}). In contrast, there were no obvious FL intensity changes after the addition of 5.0 μg mL^{-1} above common substances, indicating that the sensing strategy displayed a highly selective FL response toward paraoxon. The performance of the BChE-ATCh-MnO_2−CDs system in the presence of common existing substances was further investigated. In the presence of interfering substances (5.0 μg mL^{-1}), the nanosensor still had the same response to paraoxon (Figure 5D), which clearly suggests that the developed sensing system could provide good anti-interference capability for paraoxon detection. The selectivity of BChE-ATCh-MnO_2−CDs system for paraoxon detection was also investigated with different pesticides (the other major type of highly effective commercial pesticides) such as neonicotinoid insecticides, pyrethroid pesticides, and phenylpyrazole insecticides on the paraoxon detection. The chemical structures of these pesticides are shown in Figure S10. It can be easily observed that the typical neonicotinoid insecticides, pyrethroid pesticides, and phenylpyrazole insecticides at the concentration of 2.5 ng mL^{-1} result in negligible interferences in paraoxon monitoring (Figure S11). The above results indicated that this sensing platform showed high selectivity and good anti-interference capability for paraoxon detection.

Salt tolerance is one of the most common challenges in performing nanosensor on complex samples. Thus, we systematically studied the effect of NaCl on sensing platform. It is obviously shown in Figure S12 that the FL of BChE-ATCh-MnO_2−CDs system in the presence of 2.5 μg mL^{-1} paraoxon remains with no apparent change in the salt concentration range of 0−10.0 mmol L^{-1}, implying that the proposed system possesses good stability and outstanding ability of resisting salt. To demonstrate the applicability in detection of real samples, the established sensing system was applied for paraoxon detection in environmental and agricultural samples (tap water, river water, rice, and cabbage). For real-sample detection, pesticide was extracted from a real sample by using acetonitrile that cannot dissolve water-soluble reducing agents (glutathione, ascorbic acid, and dithiothreitol). Thus, by employing the pretreatment process (Supporting Informantion), the MnO_2 nanosheets-based platform has successfully blocked the influence of other reducing agents, obviously improving the selectivity for OPs detection. Before recovery studies, our present method and gas chromatography (GC) were utilized to test the concentration of paraoxon in these samples. The results verified that there was no paraoxon in the test samples (Table S3). The recovery test was conducted by using the standard addition method. Water samples were added with the standard solution of paraoxon. Rice and cabbage samples (10 g) were ground, then spiked with paraoxon standards. The samples were monitored by the developed platform and then confirmed by GC and another reported CDs-based sensor. As shown in Table S3, excellent recoveries between 90.6% and 106.7% with relative standard deviations (RSDs) lower than 4.3% were obtained. Furthermore, the obtained result was consistent with that of GC, suggesting the potential applicability of the proposed strategy for paraoxon detection in real samples.

CONCLUSIONS

In this study, we developed a convenient, reliable, and sensitive nanosensor for OPs detection based on the FRET between MnO_2 nanosheets and CDs. The CDs were employed as the FL units, and the MnO_2 nanosheets were used as the dual-functional nanoquencher and recognizer in this developed platform. The strategy depends on BChE-induced decomposition of MnO_2 nanosheets and OPs-caused inhibition of enzyme. Furthermore, the proposed strategy also showed visual color change in a concentration-dependent manner. With no further functionalization of MnO_2 nanosheets and CDs, the present nanosensor shows many advantages including environmental-friendliness, cost-effectiveness, and ease-of-use, demonstrating that the convenient strategy could serve as a promising platform for the on-site detection of OPs.

ASSOCIATED CONTENT

Supporting Information

The Supporting Information is available free of charge on the ACS Publications website at DOI: 10.1021/acs.analchem.7b04193.

Supplemental methods and additional data as noted in the text (PDF)

AUTHOR INFORMATION

Corresponding Authors

*E-mail for X.Y.: yanx@jlu.edu.cn.
*E-mail for X.G.S.: suxg@jlu.edu.cn.
*E-mail for Y.H.L.: yuehe.lin@wsu.edu.

ORCID

Xu Yan: 0000-0003-2152-675X
Chengzhou Zhu: 0000-0003-0679-7965
Dan Du: 0000-0003-1952-4042
Xingguang Su: 0000-0001-9856-4653
Yuehe Lin: 0000-0003-3791-7587

Author Contributions

¶(X.Y., Y.S.) These authors equally contributed to this work.

DOI: 10.1021/acs.analchem.7b04193
Anal. Chem. 2018, 90, 2618−2624

Notes

The authors declare no competing financial interest.

■ ACKNOWLEDGMENTS

This work was financially supported by the Centers for Disease Control and Prevention/National Institute for Occupational Safety and Health (CDC/NIOSH) Grant (No. R01OH011023-01A1). Its contents are solely the responsibility of the authors and do not necessary represent the official views of CDC. This work was also supported by the National Natural Science Foundation of China (Nos. 21275063 and 21575048), the Science and Technology Development project of Jilin province, China (No. 20150204010GX). X.Y. is thankful for support from the National Postdoctoral Program for Innovative Talents (BX201700096).

■ REFERENCES

(1) Pang, S.; Yang, T.; He, L. *TrAC, Trends Anal. Chem.* **2016**, *85*, 73−82.
(2) Mishra, A.; Kumar, J.; Melo, J. S. *Biosens. Bioelectron.* **2017**, *87*, 332−338.
(3) Yan, X.; Li, H. X.; Yan, Y.; Su, X. G. *Food Chem.* **2015**, *173*, 179−184.
(4) Zhang, K.; Yu, T.; Liu, F.; Sun, M.; Yu, H.; Liu, B.; Zhang, Z.; Jiang, H.; Wang, S. *Anal. Chem.* **2014**, *86*, 11727−11733.
(5) Bala, R.; Kumar, M.; Bansal, K.; Sharma, R.; Wangoo, N. *Biosens. Bioelectron.* **2016**, *85*, 445−449.
(6) Fahimi-Kashani, N.; Hormozi-Nezhad, M. R. *Anal. Chem.* **2016**, *88*, 8099−8106.
(7) Yan, X.; Li, H. X.; Wang, X.; Su, X. G. *Talanta* **2015**, *131*, 88−94.
(8) Ouyang, H.; Wang, L.; Yang, S.; Wang, W.; Wang, L.; Liu, F.; Fu, Z. *Anal. Chem.* **2015**, *87*, 2952−2958.
(9) Zhao, Y.; Zhang, W.; Lin, Y.; Du, D. *Nanoscale* **2013**, *5*, 1121−1126.
(10) Yan, X.; Li, H. X.; Yan, Y.; Su, X. G. *Anal. Methods* **2014**, *6*, 3543−3554.
(11) Wang, L. M.; Du, D.; Lu, D. L.; Lin, C. T.; Smith, J. N.; Timchalk, C.; Liu, F. Q.; Wang, J.; Lin, Y. H. *Anal. Chim. Acta* **2011**, *693*, 1−6.
(12) Hou, J. Y.; Dong, J.; Zhu, H. S.; Teng, X.; Ai, S. Y.; Mang, M. L. *Biosens. Bioelectron.* **2015**, *68*, 20−26.
(13) Teng, Y.; Jia, X. F.; Li, J.; Wang, E. K. *Anal. Chem.* **2015**, *87*, 4897−4902.
(14) Wu, Q. Q.; Fang, A. J.; Li, H. T.; Zhang, Y. Y.; Yao, S. Z. *Biosens. Bioelectron.* **2016**, *77*, 957−962.
(15) Chai, L. J.; Zhou, J.; Feng, H.; Tang, C.; Huang, Y. Y.; Qian, Z. S. *ACS Appl. Mater. Interfaces* **2015**, *7*, 23564−23574.
(16) Zhou, Y. J.; Huang, X. Y.; Liu, C.; Zhang, R. L.; Gu, X. L.; Guan, G. J.; Jiang, C. L.; Zhang, L. Y.; Du, S. H.; Liu, B. H.; Han, M. Y.; Zhang, Z. P. *Anal. Chem.* **2016**, *88*, 6105−6109.
(17) Li, X. M.; Rui, M. C.; Song, J. Z.; Shen, Z. H.; Zeng, H. B. *Adv. Funct. Mater.* **2015**, *25*, 4929−4947.
(18) Zhu, S. J.; Song, Y. B.; Zhao, X. H.; Shao, J. R.; Zhang, J. H.; Yang, B. *Nano Res.* **2015**, *8*, 355−381.
(19) Lim, S. Y.; Shen, W.; Gao, Z. Q. *Chem. Soc. Rev.* **2015**, *44*, 362−381.
(20) Li, W.; Zhang, Z. H.; Kong, B.; Feng, S. S.; Wang, J. X.; Wang, L. Z.; Yang, J. P.; Zhang, F.; Wu, P. Y.; Zhao, D. Y. *Angew. Chem., Int. Ed.* **2013**, *52*, 8151−8155.
(21) He, J. L.; Zhang, H. R.; Zou, J. L.; Liu, Y. L.; Zhuang, J. L.; Xiao, Y.; Lei, B. F. *Biosens. Bioelectron.* **2016**, *79*, 531−535.
(22) Tang, C.; Qian, Z. S.; Huang, Y. Y.; Xu, J. M.; Ao, H.; Zhao, M. Z.; Zhou, J.; Chen, J. R.; Feng, H. *Biosens. Bioelectron.* **2016**, *83*, 274−280.
(23) Li, H.; He, X.; Kang, Z.; Huang, H.; Liu, Y.; Liu, J.; Lian, S.; Tsang, C. H. A.; Yang, X.; Lee, S. T. *Angew. Chem., Int. Ed.* **2010**, *49*, 4430−4434.
(24) Fowley, C.; McCaughan, B.; Devlin, A.; Yildiz, I.; Raymo, F. M.; Callan, J. F. *Chem. Commun.* **2012**, *48*, 9361−9363.
(25) Gong, X. J.; Zhang, Q. Y.; Gao, Y. F.; Shuang, S. M.; Choi, M. M. F.; Dong, C. *ACS Appl. Mater. Interfaces* **2016**, *8*, 11288−11297.
(26) (a) Wang, Y.; Li, Z. H.; Hu, D. H.; Lin, C. T.; Li, J. H.; Lin, Y. H. *J. Am. Chem. Soc.* **2010**, *132*, 9274−9276. (b) Lin, L.; Liu, Y.; Zhap, X.; Li, J. H. *Anal. Chem.* **2011**, *83*, 8396−8402. (c) Tang, L. H.; Wang, Y.; Li, J. H. *Chem. Soc. Rev.* **2015**, *44*, 6953−6980. (d) Tang, L. H.; Chang, H. X.; Liu, Y.; Li, J. H. *Adv. Funct. Mater.* **2012**, *24*, 3083−3088.
(27) Yan, X.; Li, H. X.; Han, X. S.; Su, X. G. *Biosens. Bioelectron.* **2015**, *74*, 277−283.
(28) Li, J. M.; Li, Y. X.; Shahzad, S. A.; Chen, J.; Chen, Y.; Wang, Y.; Yang, M. D.; Yu, C. *Chem. Commun.* **2015**, *51*, 6354−6356.
(29) Zhu, C. Z.; Du, D.; Lin, Y. H. *Biosens. Bioelectron.* **2017**, *89*, 43−55.
(30) Zhu, C. F.; Zeng, Z. Y.; Li, H.; Li, F.; Fan, C. H.; Zhang, H. *J. Am. Chem. Soc.* **2013**, *135*, 5998−6001.
(31) Liao, K. H.; Lin, Y. S.; Macosko, C. W.; Haynes, C. L. *ACS Appl. Mater. Interfaces* **2011**, *3*, 2607−2615.
(32) Wei, F.; Cui, X. W.; Chen, W. X.; Ivey, D. G. *Chem. Soc. Rev.* **2011**, *40*, 1697−1721.
(33) Liu, Z. N.; Xu, K. L.; Sun, H.; Yin, S. Y. *Small* **2015**, *11*, 2182−2191.
(34) Chen, Y.; Ye, D. L.; Wu, M. Y.; Chen, H. R.; Zhang, L. L.; Shi, J. L.; Wang, L. Z. *Adv. Mater.* **2014**, *26*, 7019−7026.
(35) Deng, R. R.; Xie, X. J.; Vendrell, M.; Chang, Y. T.; Liu, X. G. *J. Am. Chem. Soc.* **2011**, *133*, 20168−20171.
(36) Ou, M.; Huang, J.; Yang, X. H.; Quan, K.; Yang, Y. J.; Xie, N. L.; Wang, K. M. *Chem. Sci.* **2017**, *8*, 668−673.
(37) Zhao, Z. L.; Fan, H. H.; Zhou, G. F.; Bai, H. R.; Liang, H.; Wang, R. W.; Zhang, X. B.; Tan, W. H. *J. Am. Chem. Soc.* **2014**, *136*, 11220−11223.
(38) Wei, C.; Yu, L. H.; Cui, C. L.; Lin, J. D.; Wei, C.; Mathews, N.; Huo, F. W.; Sritharan, T.; Xu, Z. C. *Chem. Commun.* **2014**, *50*, 7885−7888.
(39) Boppana, V. B. R.; Yusuf, S.; Hutchings, G. S.; Jiao, F. *Adv. Funct. Mater.* **2013**, *23*, 878−884.
(40) Al-Ghouti, M. A.; Al-Degs, Y. S.; Khraisheh, M. A. M.; Ahmad, M. N.; Allen, S. J. *J. Environ. Manage.* **2009**, *90*, 3520−3527.
(41) Cai, Q. Y.; Li, J.; Ge, J.; Zhang, L.; Hu, Y. L.; Li, Z. H.; Qu, L. B. *Biosens. Bioelectron.* **2015**, *72*, 31−36.
(42) Zhai, W. Y.; Wang, C. X.; Yu, P.; Wang, Y. X.; Mao, L. Q. *Anal. Chem.* **2014**, *86*, 12206−12213.
(43) Wang, Y. H.; Jiang, K.; Zhu, J. L.; Zhang, L.; Lin, H. W. *Chem. Commun.* **2015**, *51*, 12748−12751.
(44) He, D. G.; Yang, X. X.; He, X. X.; Wang, K. M.; Yang, X.; He, X.; Zou, Z. *Chem. Commun.* **2015**, *51*, 14764−14767.
(45) Yan, X.; Li, H. X.; Li, Y.; Su, X. G. *Anal. Chim. Acta* **2014**, *852*, 189−195.
(46) Zhang, W. Y.; Asiri, A. M.; Liu, D. L.; Du, D.; Lin, Y. H. *TrAC, Trends Anal. Chem.* **2014**, *54*, 1−10.
(47) Du, D.; Wang, J.; Wang, L. M.; Lu, D. L.; Smith, J. N.; Timchalk, C.; Lin, Y. H. *Anal. Chem.* **2011**, *83*, 3770−3777.
(48) Yan, X.; Li, H. X.; Hu, T. Y.; Su, X. G. *Biosens. Bioelectron.* **2017**, *91*, 232−237.
(49) Li, N.; Wang, X.; Chen, J.; Sun, L.; Chen, P. *2D Mater.* **2015**, *2*, 034018.
(50) Cui, Z.; Han, C.; Li, N. *Analyst* **2011**, *136*, 1351−1356.

DOI: 10.1021/acs.analchem.7b04193
Anal. Chem. 2018, 90, 2618−2624